APPLIED PHYSICS LETTERS **102**, 161108 (2013)

CrossMark

High speed photodetectors based on a two-dimensional electron/hole gas heterostructure

Eric M. Gallo,[1,a)] Adriano Cola,[2] Fabio Quaranta,[2] and Jonathan E. Spanier[3]
[1]*Department of Electrical and Computer Engineering, Drexel University, Philadelphia, Pennsylvania 19104, USA*
[2]*Department of Innovation Engineering, University of Salento, Lecce, Italy*
[3]*Department of Materials Science and Engineering, Drexel University, Philadelphia, Pennsylvania 19104, USA*

(Received 27 November 2012; accepted 7 April 2013; published online 23 April 2013)

We report on high-speed metal-semiconductor-metal (MSM) resonant cavity enhanced photodetectors based on Schottky-contacted (Al,In)GaAs heterostructures containing both electron and hole quantum wells. Interdigitated detectors were fabricated and characterized with and without an underlying Distributed Bragg Reflector (DBR). All detectors had very low dark currents and high linear responsivities. The fastest measured temporal response with a 16 ps full-width at half-maximum and a 29 ps fall time was demonstrated on a device with 1 μm gap between electrodes and an underlying DBR. Single quantum well detectors have previously demonstrated increased responsivity and speed but were limited by a slow decaying tail in the high speed photoresponse, attributed to the long collection path of minority carriers. The use of an electron and hole well, separated by a 110 nm absorption region as well as an underlying DBR, eliminates the slow tail by providing an enhanced collection path for both optically generated electrons and holes. Here, we present the fabricated device structure along with the DC and high speed photoresponse under varying incident powers. We briefly compare these results to those of the previous single well devices and attribute improvements in the time response tail to enhanced diffusion created by the presence of the separated dual well structure. © *2013 AIP Publishing LLC*
[http://dx.doi.org/10.1063/1.4802595]

Metal-semiconductor-metal (MSM) devices based on GaAs offer a simple and effective geometry for high speed photodetection, providing high responsivity and wavelength selectivity with the incorporation of an underlying Distributed Bragg Reflector (DBR)[1,2] while allowing monolithic incorporation into integrated circuits, creating detector and receiver circuitry on a single chip.[3] The performance of these devices can be further enhanced by introducing heterostructures to reduce dark currents and low frequency gain[4–6] and δ-doping to increase speed.[5,7,8] Bandwidths of these detectors are typically constrained by slow decaying tails in the high speed response attributed to minority carriers.[5,8] Heterostructures and δ-doping create built-in vertical electric fields that separate optically generated electron-hole pairs, improving majority carrier collection while pushing the minority carriers deeper into the device and increasing travel paths to electrodes. Additionally, the use of Schottky contacts results in applied potentials dropping entirely across the contacts, leaving little to no lateral electric field in the channel.[8]

Several research groups have explored methods to mediate the effects of minority carriers while maintaining the other high performance metrics of MSM detectors. Incorporating an underlying DBR simultaneously increases the responsivity while blocking electron-hole pairs from beneath the absorption region from participating in the measured response.[1,6] Low temperature grown GaAs has been incorporated into heterostructures to create regions of short carrier lifetimes, removing slow minority carriers through recombination.[9,10] Creating p-type detectors has been shown to improve the response, by placing the much faster electron into the minority carrier role.[5,11]

To date, research has centered on single quantum well high speed detectors. Here, we present results on the use of a dual well structure (2DEHG) for high speed detection. Several research groups have previously explored the electrical properties of opposite polarity quantum wells separated by a wide band gap barrier, investigating physical phenomena such as Coulomb drag.[12] In our study, a 110 nm GaAs absorption region separates a δ-doped electron and hole well, creating high mobility 2D sheets of both electrons and holes within the device. DC and high speed optical performance was characterized on detectors with an underlying DBR (DBR+) and without (DBR−). The results are then briefly compared with the previous single well detectors. Dual well devices with a DBR are shown to eliminate the slow decaying tail seen in single well MSM devices, even at higher incident powers.

Fig. 1(a) provides a schematic cross section of the 2DEHG structure grown by MOCVD (metalorganic chemical vapour deposition) on a semi-insulating (SI) GaAs substrate. The top barrier layer consists of $Al_{0.3}Ga_{0.7}As$ (56.4 nm) and a $6 \times 10^{12}/cm^2$ Si δ-doping layer separated by 5 nm from the GaAs absorption layer (109.4 nm), creating an electron well at the interface. Beneath the GaAs absorption layer is an 8 nm pseudomorphic $In_{0.2}Ga_{0.8}As$ layer creating the hole well, populated by a $2.5 \times 10^{12}/cm^2$ C δ-doping layer located 5 nm below in a lower barrier formed by

[a)]Email: eric.m.gallo@drexel.edu

 © 2013 AIP Publishing LLC

$Al_{0.3}Ga_{0.7}$ As (57.3 nm). This is followed by a DBR consisting of 15 pairs of quarter wave $Al_{0.3}Ga_{0.7}As/AlAs$ layers (55.3 nm/71.1 nm) on a SI GaAs substrate for DBR+ and immediately by the substrate in DBR−.

Detectors were fabricated by initially depositing a 200 nm silicon nitride (Si_3N_4) isolation layer and subsequently opening 40 μm × 40 μm windows with reactive ion etching (RIE). Interdigitated Schottky contact finger electrodes, Ti/Pt/Au (30 nm/30 nm/60 nm), were patterned within the windows, along with contact pads on top of the Si_3N_4 via e-beam evaporation. The resulting detectors are mesa isolated and have finger widths of 2 μm, gaps between fingers of 1, 2, and 4 μm and 150 μm × 80 μm contact pads. Structures were simulated using a 1D Poisson/Schrodinger solver,[13] the results of which are shown in Fig. 1(b), assuming a Schottky contacted surface. The Fermi level location indicates that wells may not be fully populated in dark conditions. The presence of the DBR has only minor effects on the band structure of the upper active layers. Simulated band structure was confirmed by measured photoluminescence, shown in Fig. 1(c). Expected peaks corresponding to carriers in the InGaAs layer (1.29 eV, 1.33 eV) and carriers in the GaAs absorption layer (1.42 eV) are clearly seen, along with a peak near 1.5 eV in DBR+ arising due to photoluminescence enhancement in the presence of DBR. The results indicate the high quality of the as-grown material.

DC device characteristics were measured using a parameter analyzer and probe station. For time response measurements, the photodetectors were illuminated by 80 fs pulses from a tunable Ti:sapphire laser, operating at a 830 nm center wavelength and a 76 MHz repetition rate. The response was measured using 60 GHz microwave probes coupled to a 50 GHz oscilloscope. Traces shown were taken at 10 V bias and under powers from μW to mW, measured as DC. The pulsed beam was directed in free space incident on devices under test and defocused to illuminate the entire active area.

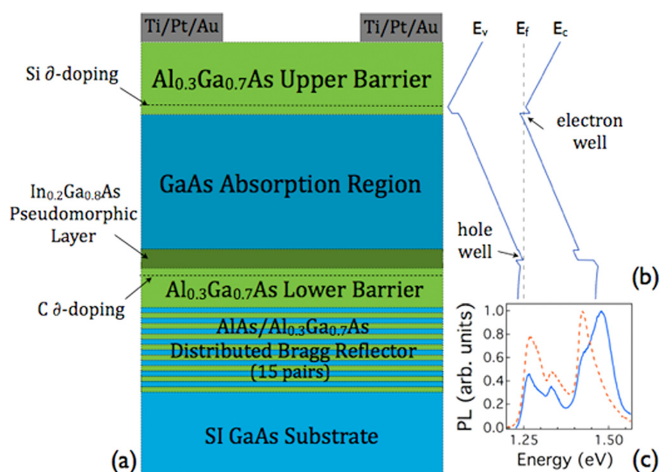

FIG. 1. (a) Cross section of 2DEHG wafer with built in DBR, indicating δ-doping layers and contacts. (b) Simulated band structure of the 2DEHG, arrows indicate the location of each well. (c) Photoluminescence signal from substrates with an underlying DBR (solid) and without (dashed) at room temperature. Incident excitation wavelength and intensity are 488 nm and approximately 20 mW/cm^2, respectively.

Most devices showed dark currents near 100 pA at 10 V applied bias. Leakage through the Si_3N_4 isolation layer was below measurable levels for our instruments (<100 fA). Current-voltage measurements under CW illumination showed the onset of saturation near 2 V in both structures with DBR− exhibiting a current increase again above 5 V. This increase may be attributed to the onset of carrier collection within the substrate, which is otherwise blocked by the wide band gap DBR. All devices showed a linear increase in response with power and with rough estimates of responsivity between 10 and 15 mA/W. The photocurrent wavelength response of DBR+ showed enhanced photoresponse centered at 830 nm with a 46 nm FWHM.

Fast temporal response was measured for 12 different detectors with different gap widths. Fig. 2 provides typical normalized responses from devices with gap widths of 2 μm under varying incident powers (830 nm). DBR+ showed a strong response that quickly decays to zero for all powers, 88 ps at 69 μW to 239 ps at 14 mW. DBR− showed a considerably slower response. At lower powers, the response is similar in shape to that of DBR+ but with increased fall times (>500 ps). At higher powers, however, a knee emerges, bending into a long tail as the signal falls below 20% of its peak, extending fall times to near 1 ns. The inset in Fig. 2(a) plots the change in FWHM times for both devices as a function of incident power, demonstrating the faster response of DBR+ and also indicating the change in response shape at higher energies. Changes in fall times to 5% of peak are plotted in the inset of Fig. 2(b), showing the rapid increase in the slow tail with increasing power in DBR− while DBR+ appears to saturate near 300 ps. The fall time to 5% of peak is used as a metric to ensure the effects of the slow tail are included, which can be disguised in typical 10% fall time measurements. Including a DBR

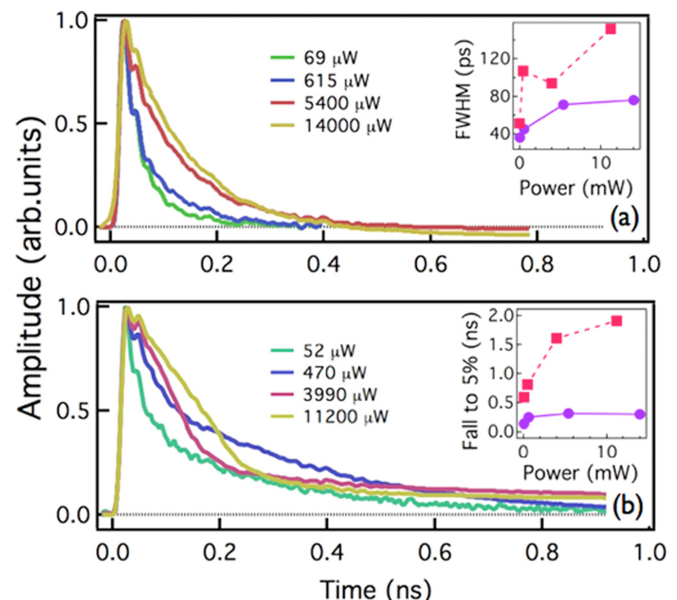

FIG. 2. (a) Normalized high speed response of detector with an underlying DBR for four incident powers at 10 V bias and 830 nm (b) Normalized high speed response of device without an underlying DBR for four separate powers at 10 V and 830 nm. FWHM values and the fall times to 5% of maximum are shown in insets (a) and (b), respectively, for DBR+ (solid) and DBR− (dashed).

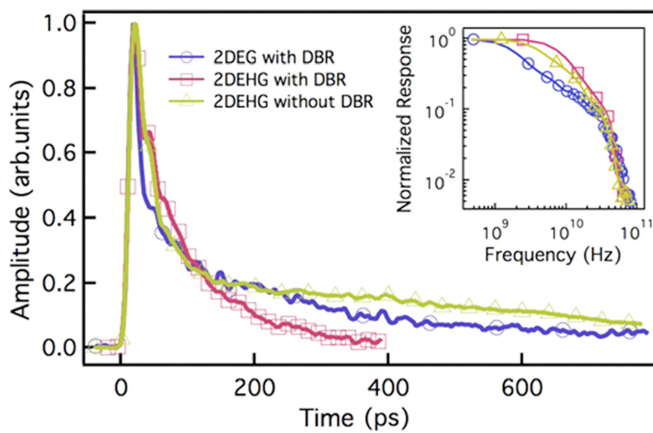

FIG. 3. High speed response of 2 μm gap devices at 10 V bias and 1 mW incident power. Normalized frequency response of the traces shown is provided in the inset.

consistently increased the peak amplitude of the response close to three times compared to devices without showing no sign of a slow decaying tail even at high incident powers. This behavior was seen at all gap widths. Increasing the applied bias further reduced the FWHM and fall times of devices, while increasing the gap width increased fall time values. DBR+ devices with gap widths of 1 μm produced the fastest performance, demonstrating FHWM values of 16 ps and fall times of 29 ps at 82 μW of incident power. The 16 ps FWHM approaches the limit of the measurement setup, indicating some of the time response may be dominated by the probes and oscilloscope. External quantum efficiency is estimated at 16.7%.[18]

To evaluate the effects of the dual quantum well structure, we compared these devices to the previous results on single well devices (2DEG). The lack of equivalent measurement conditions made rigorous comparison difficult but obvious trends can be seen in the available data. Fig. 3 compares the temporal responses from a representative 2DEG with the 2DEHG results at 10 V bias, incident powers near 1 mW, gap widths of 2 μm, and identical device geometry. The DBR+ shows a faster response and no observable slow decaying tail, returning to zero in 300 ps. The response of the 2DEG and DBR− have not reached zero at 600 ps. 2DEHG with DBR devices consistently demonstrated a larger peak response and an absence of the long tail seen in 2DEG detectors. However, without an underlying DBR, 2DEHG devices provided the longest fall times and FWHM values. The inset of Fig. 3 provides the frequency response of the three detectors, again confirming the higher speed of 2DEHG with DBR devices.

The results demonstrate increased performance resulting from both an underlying DBR and the incorporation of a dual quantum well structure. The simulation work presented in Ref. 8 showed that under applied bias, the potential drop in the presence of an underlying δ-doped quantum well fell almost entirely across the reverse biased Schottky contact in the MSM structure, leaving no lateral electric field to create drift within the channel and wells. As a result, diffusion becomes the dominant current mechanism away from the contacts in regions not depleted by the electrode interfaces.[14] An incident optical pulse generates electron-hole pairs that are immediately separated by the built in field within the absorption layer, moving electrons to the top well and holes into the bottom well, increasing local carrier concentrations and preventing recombination. Carriers generated near contacts in depleted regions are swept up and collected quickly while remaining carriers must diffuse toward their respective contacts. The 2DEHG structure enhances diffusion by increasing local concentrations of both carriers and increasing the mobility of holes by moving them to the pseudomorphic InGaAs layer. The overall effect is to increase both collection efficiency and speed of the device. Similar effects have been observed in p-i-n detectors[15] and in exciton diffusion in quantum well structures.[16,17] Previous quantum well detectors reported were dominated by collection near the contacts, explaining the small change in response times seen between varying gap widths, while the introduction of the dual well structure enhances collection within the channel increasing responsivity and eliminating the slow decaying tail.

We have demonstrated high speed optical detectors at 830 nm based on a separated dual quantum well device. 2DEHG detectors with an underlying DBR had a best result of 16 ps FWHM and 29 ps fall time for 1 μm wide channels, limited by the bandwidth of the measurement system. The introduction of the dual well structure eliminated the slow decaying tail seen in single well devices when combined with an underlying DBR. The measurements indicate that there is a significant performance enhancement due to both the underlying DBR and the 2DEHG structure.

The authors would like to thank B. Nabet for discussions on the 2DEHG design, M. Currie for assistance in the high speed optical measurements, and M. Sipics for assistance in manuscript preparation. E.M.G. was supported by an NSF GK-12 Graduate Fellowship during this work. E.M.G. and J.E.S. acknowledge support, including instrumentation, from the ARO under W911NF-08-1-0067.

[1]M. S. Unlu and S. Strite, J. Appl. Phys. **78**, 607–639 (1995).
[2]B. M. Onat, M. Gokkavas, E. Ozbay, E. P. Ata, E. Towe, and M. S. Unlu, IEEE Photonics Technol. Lett. **10**, 707–709 (1998).
[3]C. Moglestue, J. Rosenzweig, J. Kuhl, M. Klingenstein, M. Lambdorff, A. Axmann, Jo. Schneider, and A. Hulsmann, J. Appl. Phys. **70**, 2435–2448 (1991).
[4]A. Anwar and B. Nabet, IEEE Trans. Microwave Theory Tech. **50**, 68–71 (2002).
[5]J.-I. Chyi, Y.-J. Chien, R.-H. Yuang, J.-L. Shieh, J.-W. Pan, and J.-S. Chen, IEEE Photon. Technol. Lett. **8**, 1525–1527 (1996).
[6]S. Collin, F. Pardo, S. V. Averin, N. Bardou, and J.-L. Pelouard, Quantum Electron. **40**, 421–424 (2010).
[7]X. Chen, B. Nabet, F. Quaranta, A. Cola, and M. Currie, Appl. Phys. Lett. **80**, 3222–3224 (2002).
[8]X. Zhao, M. Currie, A. Cola, F. Quaranta, E. Gallo, J. E. Spanier, and B. Nabet, IEEE Trans. Electron Devices **55**, 1762–1770 (2008).
[9]M. Currie, F. Quaranta, A. Cola, E. M. Gallo, and B. Nabet, Appl. Phys. Lett. **99**, 203502 (2011).
[10]S. Y. Chou, Y. Liu, W. Khalil, T. Y. Hsiang, and S. Alexandrou, Appl. Phys. Lett. **61**, 819–821 (1992).
[11]B. Nabet, A. Cola, X. Chen, and F. Quaranta, IEEE Trans. Microwave Theory Tech. **51**, 2063–2072 (2003).
[12]H. Rubel, A. Fischer, W. Dietsche, K. v. Klitzing, and K. Eberl, Mater. Sci. Eng., B **51**, 207–211 (1998).
[13]G. Snider, 1D Poisson (version beta 8j) [computer software] (2007).
[14]L.-C. Liou and B. Nabet, Appl. Opt. **35**, 15–23 (1996).

[15]H. Schneider, E. C. Larkins, J. D. Ralston, J. Fleissner, G. Bender, and P. Koidl, Appl. Phys. Lett. **60**, 2648–2650 (1992).
[16]Z. Vörös, R. Balili, D. W. Snoke, L. Pfeiffer, and K. West, Phys. Rev. Lett. **94**, 226401 (2005).
[17]Y. Takahashi, K. Muraki, S. Fukatsu, S. S. Kano, Y. Shiraki, and R. Ito, Jpn. J. Appl. Phys., Part 1 **32**, 5586–5590 (1993).
[18]The calculation of external quantum efficiency assumed a 56 μm laser spot diameter and 40 μm $\times$ 40 μm device area (including gaps and fingers). Quantum efficiency was determined by evaluating the incident photons in a single pulse at 830 nm and comparing that value to the integrated high speed response, assuming the measured signal dropped across a bias-T with a characteristic impedance of 50 Ω.